Mesoporous NanocrystallineTiO_2 Supported Metal (Cu, Co, Ni, Pd, Zn, and Sn) Catalysts: Effect of Metal-Support Interactions on Steam Reforming of Methanol

Vishwanath G. Deshmane[a,b], Sri Lanka Owen[a], Richard Abrokwah[c], andDebasishKuila[a]*

[a]Department of Chemistry, Greensboro, NC 27411 USA

[b]Department of Chemical, Biological and Bioengineering , Greensboro, NC 27411 USA

[c]Department of Energy and Environmental Systems, North Carolina Agricultural and Technical State University, Greensboro, NC 27411 USA

*To whom correspondence should be addressed.

Phone: (336)285-2243. Fax: (336)334-7124.

E-mail: dkuila@ncat.edu

Abstract

Mesoporous TiO_2supported Cu, Co, Ni, Pd, Sn and Zn catalysts (M-TiO_2) were synthesized using facile one-step synthesis method and were characterized using BET, XRD, TGA-DSC, TEM, SEM-EDX, ICP-OES, and H_2-TPR studies. The catalysts were further tested for steam reforming of methanol (SRM)to investigate their comparative catalytic performance. Depending on the nature of the metal component, the catalysts exhibited surface area, pore sizes, and TiO_2 crystallite sizes in the range of 99-309 m^2/g, 2.63-4.69 nm and 6.8-17.2 nm, respectively.N_2-physorption,TGA-DSC and XRD analysis demonstrated that the presence of metal in the TiO_2 matrix stabilized the mesoporous structure by hindering the crystal growth during heat treatment and thereby preventing the collapse of porous structure.Furthermore, the characterization of 5-20%Zn-TiO_2 catalysts indicated that there exist an optimum Zn loading to obtain highest surface area which was found to be 15% in the present study giving a high surface area of ~258 m^2/g. This was consistent with theSRM studies where the activity increasedup to 15% and then decreased significantly with further increase in Zn loading to 20%. The results of the SRM studies coupled with extensive TPR analysis of different M-TiO_2 catalysts suggest that the specific metal-support interactions play a crucial role in controlling its performance on H_2 production. The SRM activity order for different metals incorporated in mesoporous TiO_2 was observed to be:Pd> Ni > Zn > Co >> Cu >> Sn. The Zn-TiO_2 catalyst showed the lowest CO selectivity among the different catalysts studied.

Keywords: Mesoporous TiO_2; Porous Structure Stabilization; Metal-support Interactions; Cu, Co, Ni, Pd, Sn, Zn-TiO_2; TPR; Hydrogen Production; Steam Reforming.

1. Introduction

The increasing global energy demand and environmental crisis due to incessant use of fossil fuels has stimulated research for a clean and efficient source of energy for both mobile and stationary applications in the form of fuel cells[1, 2]. Proton exchange (also called polymer electrolyte) membrane fuel cells (PEMFC) which mainly use hydrogen (H_2) as fuel are considered to be the most promising among different types of fuel cells[3-5]. Therefore,H_2 is likely to play a crucial role in the energy portfolio of future in the form of H_2 economy. Although hydrogen is potentially an ideal energy carrier, it is extremely difficult to store and transport. The effective exploitation of H_2 as an energy carrier will need a massive development in storage, transportation and distribution infrastructure. Thus, the production of hydrogen *insitu* using an on-board steam reformer for fuel cells in various transportation applications is a subject of great interest in the scientific community[6].Not only it can eliminate the hydrogen storage and transportation safety concerns but allowsthe use of present gasoline distribution infrastructure for supply of reforming feed-stocks such as methanol and ethanol. However, in order for on-board H_2 production to be a reality, development of economical, effective and efficient steam reforming catalysts is one of the important challenges that still need to be addressed.

The nature of support material and its physical state strongly influence the activity and selectivity ofsteam reforming reactions. A wide range of support materials have been investigated for steam reforming reactions including Al_2O_3, ZrO_2, CeO_2, Y_2O_3, La_2O_3, ZnO, TiO_2 and MgO[7-9].A careful review of the literature shows that,although TiO_2 has been used extensively in photo-catalysis for photo-degradation of various pollutants and is well known for its unique metal-support interactions showing excellent catalytic properties [10-12],limited comprehensivestudies have been reported forTiO_2supportedmetal catalysts in hydrogen

production via steam reforming reactions [13-17]. More specifically, the influence of metal-support interactions on steam reforming activity and selectivityhas not been studied in detail.Pinzari et al. [13]synthesized Zn/TiO_2 catalysts using impregnation methodthat yielded surface area in the range of ~15-80 m^2/g depending on Zn loading. The highest activity was obtained with 5%Zn at 400 °C.Nichele et al. [14] investigated the Ni/TiO_2 catalysts prepared by two routes involving impregnation of$Ti(OH)_4$ and TiO_2.Both, the preparation method and calcination temperature strongly influenced the catalyst properties (surface area 2-82 m^2/g)and subsequent ethanol steam reforming activity due to their pivotal role in establishing the strong-metal-support-interactions (SMSI). In theirmost recent studies[15],they compared the performance of Ni, Co and Cu metals supported on $TiO_2$for ethanol steam reforming.Ni/TiO_2 showed significantly higher activity compared to Co/$TiO_2$and Cu/TiO_2. The highest activity of Ni was attributed to its ability of C-C bond cleavage. The tendency of Ni deactivation due to coke formation was shown to be significantly controlled by tuning the interactions between Ni and TiO_2 via catalyst preparation.Thus, in addition to the nature of support material, the catalyst preparation method [18, 19] and type of the active metal component[20-22]can have profound influence on steam reforming performance of catalysts.

In order to have a better understanding of the metal-support interactions, we have synthesized metal nanoparticles supported onhigh surface area mesoporous TiO_2 catalysts using facile one-step procedure developed in our laboratory.Six metal components - Cu, Co, Ni, Pd, Sn and Zn, reported to be active for steam reforming reactions, were incorporated in mesoporous TiO_2 to obtain different M-TiO_2 catalysts. These catalysts were extensively characterized by different techniques including temperature programmed reduction (TPR) studies and tested for steam reforming of methanol (SRM) to understand the comparative role of different metals and

their interactions with TiO_2 on reaction activity and selectivity. To the best of our knowledge, no such systematic studies have been reported using one-step synthesis of high surface area mesoporous TiO_2supported Cu, Co, Ni, Pd, Sn and Zn catalysts.

2. Experimental

2.1. Materials and Methods

Titanium (IV) isopropoxide, 98+% (TIPR) and ammonium hydroxide, reagent ACS were obtained from Acros Organics, New Jersey, USA. Hexadecyltrimethylammonium bromide minimum, 99% (CTAB), Cu (II) nitrate hydrate, 98% ACS reagent,cobalt (II) chloride hexahydrate, zinc nitrate hexahydrate 98%, tin chloride dehydrate 98%, and palladium nitrate hydratewere procured from Sigma-Aldrich, Missouri, USA. Nickel nitrate, hydroflouricacid, ethanol anhydrous and acetone, ACS reagent were purchased from Fischer Scientific, New Jersey, USA. All materials used were analytical grade and used without further purification. The water used at all stages of the experiments was purified using a Mill-Q Advantage A10 with Elix 5 system obtained from Millipore Corporation (Bedford, MA, USA).

2.2. Experimental Procedure

Mesoporous TiO_2 containing metal particles, M-TiO_2,(M: Cu, Co, Ni, Pd, Sn, and Zn) were synthesized using the reactants molar ratio of 1 TIPR: 0.52 CTAB: 282 H_2O: 26.21 ethanol. Several preliminary experiments were carried out to finalize most favorable synthesis parameters and procedure reported in this study. The quantities of the metal precursors used were determinedto obtain 10wt% loading for different M-TiO_2catalysts and 5-20wt% loading for Zn-TiO_2.While the % metal loading refers to the wt% loading, TiO_2 denotes the mesoporous TiO_2 in rest of this article. In a typical synthesis, a measured quantity of CTAB was added to a water-ethanol solution with 4/1 (water/ethanol) volumetric ratios and stirred for 30 min to get a clear

solution. In another beaker, a solution of metal salt in ethanol was prepared. After stirring for 30 min, this solution was mixed with CTAB solution and stirred again. To the resulting solution, a measured quantity of TIPR was added slowly and drop-wise with continuous vigorous stirring. The stirring was continued for another 30 min after TIPR addition. Then NH_4OH was added drop-wise to adjust the pH of solution to ~10. The resulting mixture was stirred for 24 h at room temperature. The precipitate was washed with water until the pH of filtrate reached close to 7. The precipitate was then washed with ethanol and filtered. The filtered material was air dried for 24 h followed by oven drying at 110 °C for 24 h. Finally, the dried material was calcined at 350 °C for 5 h with a heating and cooling rate of 2 °C/min to remove the traces of templating material and to obtain crystalline TiO_2.

2.3. Catalyst Characterization

The catalysts were extensively characterized to study their physical and chemical properties using different techniques including N_2physisorption, small and wide angle X-ray diffraction (XRD), thermo-gravimetric and differential scanning calorimetric analysis (TGA-DSC), transmission electron microscopy (TEM), scanning electron microscopy (SEM), energy dispersive X-ray spectroscopy (EDX), inductively coupled plasma optical emission spectroscopy (ICP-OES), and temperature programmed reduction (TPR).

TGA–DSC of the different catalyst samples under air flow (100 ml/min) was carried out using SDT Q600 V20.4 Build14 system (TA instruments, New Castle, DE, USA). The as-prepared catalyst sample was placed in an alumina crucible and heated under air at 10 °C/min from ambient to desired temperature.N_2 adsorption-desorption technique was used to determine Brunauer-Emmett-Teller (BET) surface area, pore size and pore volume of the catalysts samples. The N_2 adsorption/desorption isotherms were measured at liquid nitrogen temperature of -196.14

°C using Quantachrome NOVA 2200e instrument (Quantachrome Instruments, Boynton Beach, FL, USA).Samples were thoroughly degassed at 150 °C for several hours before the adsorption measurements. The total pore volume was derived based on the amount of N_2 adsorbed at a relative pressure close to one.Barrett-Joyner-Halenda (BJH) method was applied to the desorption branch of N_2 isotherms to determine the pore size distribution (PSD) and average pore diameters [23].

Powder XRD patterns of the catalyst samples were obtained using D8 DISCOVER X-ray diffractometer from Bruker (Bruker Optics, Inc., Billerica, MA) equipped with a PSD detector using Cu Kα radiations generated at 40 mA and 40 kV at 0.014°/s scan speed.Scherrer's formula (**Eq.(1)**) was used to determine the sizes of TiO_2 and metal crystallites from full-width-half-maximum of respective XRD peaks.

$$\tau = \frac{0.9\lambda}{\beta \cdot \cos\theta} \quad (1)$$

The actual elemental composition of the calcined catalysts was determined by an ICP-OES (Agilent 710-ES) technique.A mixture of 2 ml hydrofluoric acid (51%) and 3 ml nitric acid (68%) was used to dissolve the 75 mg catalyst sample at 80 °C.Fourier transform infrared (FTIR) measurements were recorded on KBr pellets with Shimadzu IR Prestige-21 Fourier transform infrared (FTIR) 8300 spectrometer equipped with mercury-cadmium-telluride (MCT) detector.Zeiss Libra 120 (©Carl Zeiss NTS GmbH, Oberkochen, Germany) instrument operating at 120 kVwas used to obtain the high resolution transmission electron microscopy (HRTEM) images of the catalyst samples. For the analysis, the catalyst sample particles were dispersed in ethanol with the help of ultrasonication and then dropped onto a holey-carbon-coated copper microgrid.Elemental mapping showing the dispersion of different metals in the M-TiO_2 catalysts was carried out on Zeiss EVO LS10 SEM equipped with OXFORD INCA X-act detector. For

the analysis,powdered samples were mounted on aluminum stubs with the help of two sided carbon tape. H_2-TPR experiments were performed on AutoChem II 2920 Chemical Analyzer equipped with thermal conductivity detector (TCD) from Micromeritics Instrument Corp. (Norcross, GA, USA).Prior to TPR analysis, the catalyst were degassed at 200 °C for 30 min in Argon (Ar) stream. The TPR profiles were recorded in the flow of 10%H_2/Ar gas mixture at 50 ml/min, and the temperature was raised up to 900 °C with a heating rate of 10 °C/min.

2.4. Catalysts Testing

Methanol steam reforming experiments to examine the performance of different TiO_2supported catalysts were carried out in a tubular stainless steel packed bed reactor (6.22 mm internal diameter)in the range of 150-350 °C. A catalyst and sand (white quartz, 50-70 mesh) mixture (2:1 volume ratio) was packed into the reactor with quartz wool placed at both ends. The calcined catalyst was first reduced *ex-situ* in a tubular furnace for 2 h and then *in-situ* in the reactor for 1 h using 4% H_2/Arat 350 °C.A methanol/water mixture was fed to the reactor using aHPLC pump via a vaporizer set at 350 °C.The reactor outlet stream was passed through a condenser to separate unreacted reactants from the non-condensable product gases.While the reaction temperature was varied in the range of 150–350 °C, gas hourly space velocity (GHSV) and methanol to water mole ratio were kept constant at 2838 h^{-1} and 3:1, respectively, for all the experiments.The reaction products and collected condensate were analyzed by Agilent 7890B gas chromatography system. The gaseous products were separated using RestekShinCarbon (2 m x 2 mm x 1/8”) packed column and analyzed on thermal conductivity detector (TCD) using Argon as a carrier gas. Condensate mixture carried using He gas was separated on Agilent DB-1 (60 m x 250 µm x 1 µm)capillary column and analyzed on flame ionization detector (FID). While the conversion of methanol isobtainedusing methanol material balance based on feed and

condensate (**Eq.(2)**), the productselectivitiesare determined by hydrogen (**Eq.(3)**) and carbon (**Eq.(4)**) balance among the different non-condensable products.

$$X_{Methanol} = \frac{CH_3OH\ moles\ converted}{CH_3OH\ moles\ fed} \times 100\% \quad (2)$$

$$S_{H_2} = \frac{H_2\ moles\ in\ product}{H_2\ moles\ in\ product + 2 \times CH_4\ moles\ in\ product} \times 100\% \quad (3)$$

$$S_{CO/CO2/CH4} = \frac{CO/CO2/CH4\ moles\ in\ product}{(CO_2 + CO + CH4)\ moles\ in\ product} \times 100\% \quad (4)$$

3. Results and Discussion

3.1. Thermal and Calorimetric Analysis of M-TiO_2Samples

Fig. 1a shows the representative TGA-DSC profiles of TiO_2 and 10%Co-TiO_2 recorded in air.TGA profiles for both the samples showed two weight loss stages. The first one is located below 200 °C and is associated with an endothermic peak centered at ~85 °C. This weight loss is attributed to the removal of adsorbed water on the surface of TiO_2. The second weight loss observed in the range of 200 to 400 °C coincided with an exothermic peak between 220-300 °C in the DSC profile and is due to the exothermic decomposition of CTAB which was used as the templating agent.In addition,10%Co-TiO_2 sample showed a second small exothermic peak at about 300 °C that is ascribedto the decomposition of metal precursor (in this case, $CoCl_2$) [24].The exothermic peaks of the DSC profilescentered at ~450 °Cand ~510 °C, both associatedwith insignificant weight loss, observed for TiO_2 and 10%Co-TiO_2, respectively,are attributed to the phase change of TiO_2 fromamorphous to crystalline state[25]. It can be further noticed that the crystallization temperatureof TiO_2increased from ~450 to ~500 °C upon addition of cobalt.

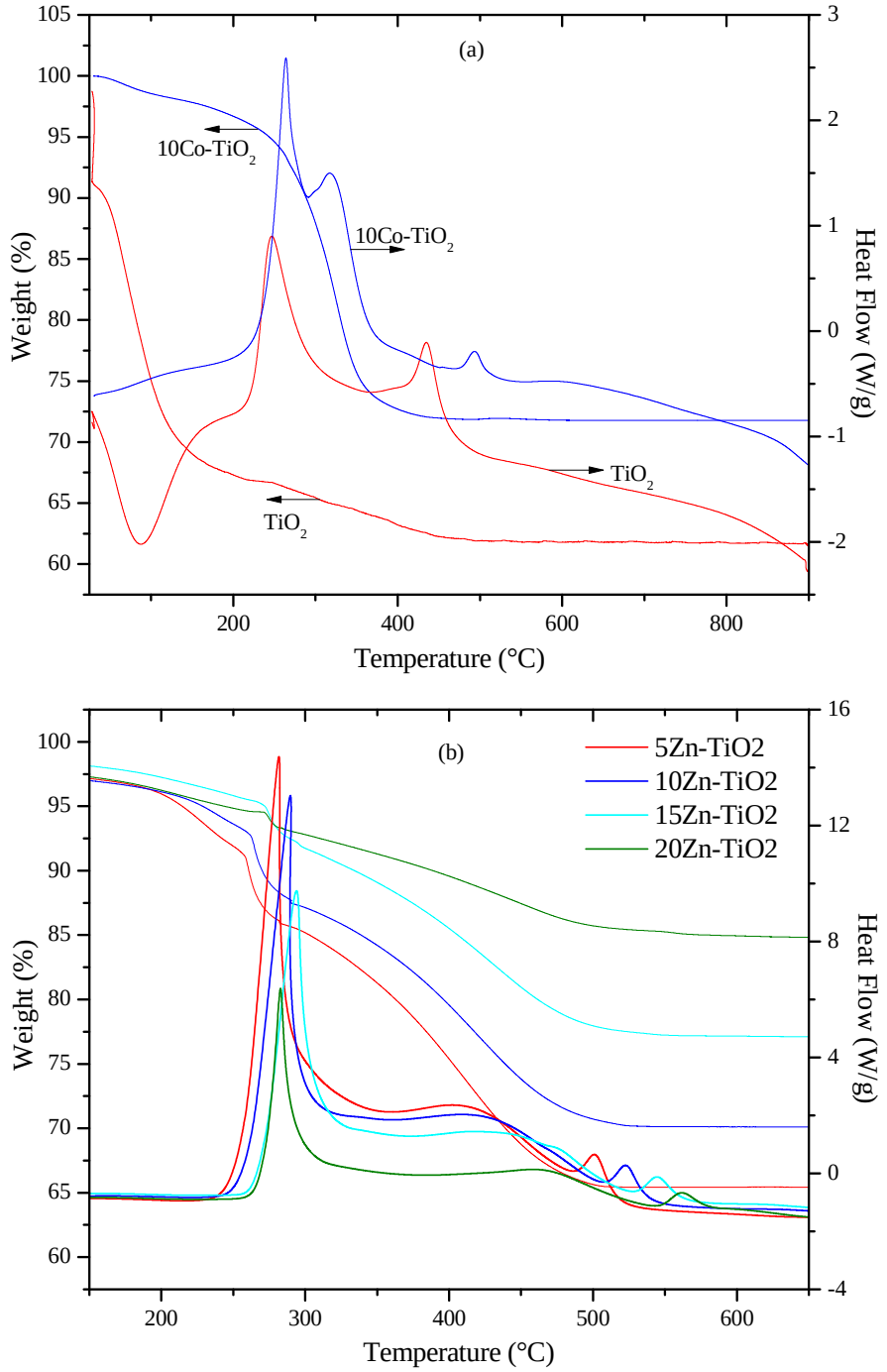

Fig. 1.TGA-DSC profiles of (a) TiO_2 and 10%Co-TiO_2 and (b) 5-20%Zn-TiO_2 catalyst samples

The TGA-DSC profiles of different Zn-TiO_2 catalysts with 5-20% Zn loading are shown **Fig. 1b**. The general behavior of the profiles is similar to that described in **Fig. 1a**. However, two conspicuous features were observed in**Fig. 1b**;first, aconsistent decrease in the intensity of

exothermic peak in the range of 240-340 °C and second, a shift in the crystallization temperature to higher values with increase in the Zn loading. The Zn-TiO_2 sample with 5% loading has a crystallization temperature of~500 °C, which increased to ~560 °C with 20% loading. The decreased peak intensity at higher Zn loading indicates the presence of lower CTAB in the as-prepared samples due to its replacement by Zn. The consistent delay in the crystallization temperature of TiO_2 with increase in Zn loading will be discussed in more detail in the subsequent sections (3.2 and 3.3).

3.2. X-ray Diffraction Analyses of Different M-TiO_2 Catalysts

Fig.2 presents the XRD patterns of different calcined M-TiO_2 samples. TiO_2 exists in three different crystalline phases:rutile (tetragonal), anatase (tetragonal), and brookite (orthorhombic).

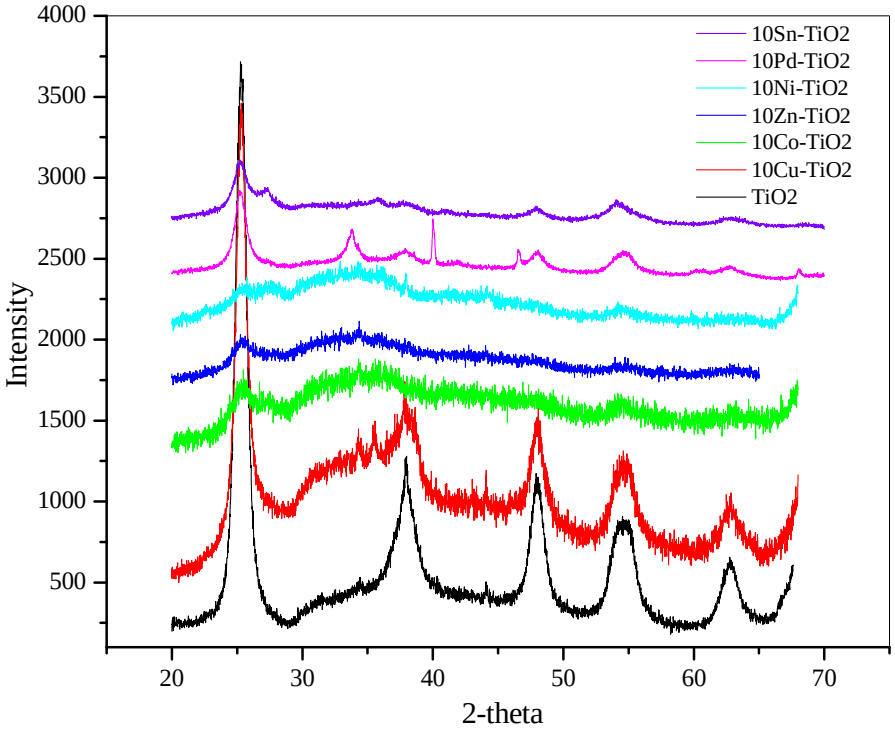

Fig. 2. X-ray diffraction patterns for different M-TiO_2 catalyst samples.

The XRD pattern of TiO_2 clearly shows well-resolved, sharp peaks at 25°, 38°, 48°, 55°, 63° corresponding to the (101), (004), (200), (105), and (211) diffraction planes, respectively, of

anatase structural phase (JCPDS# 21-1272). However, addition of a metal led to a decrease in intensity of these peaks, indicating a lower degree of crystallinity. This decrease in crystallinity appeared to strongly dependon the type of metal incorporatedin TiO_2. For example, while the additionof Cu showed no significant change in intensities, the presence of Ni yielded very low intensity broad peaks corresponding to the anatase phase. The XRD spectrum of 10%Cu-TiO_2 exhibits two peaks at 2-theta 35.5° and 38.7°, ascribed to the CuO crystal phase, assigned to (002) and (111) planes (JCPDS# 80-1917), respectively. The XRD spectrum of 10%Pd-TiO_2showed peaks at 2-theta values of 33.6° and 42° assigned to (002) and (110) crystalline planes, respectively, oftetragonal PdO(JCPDS# 75-584).

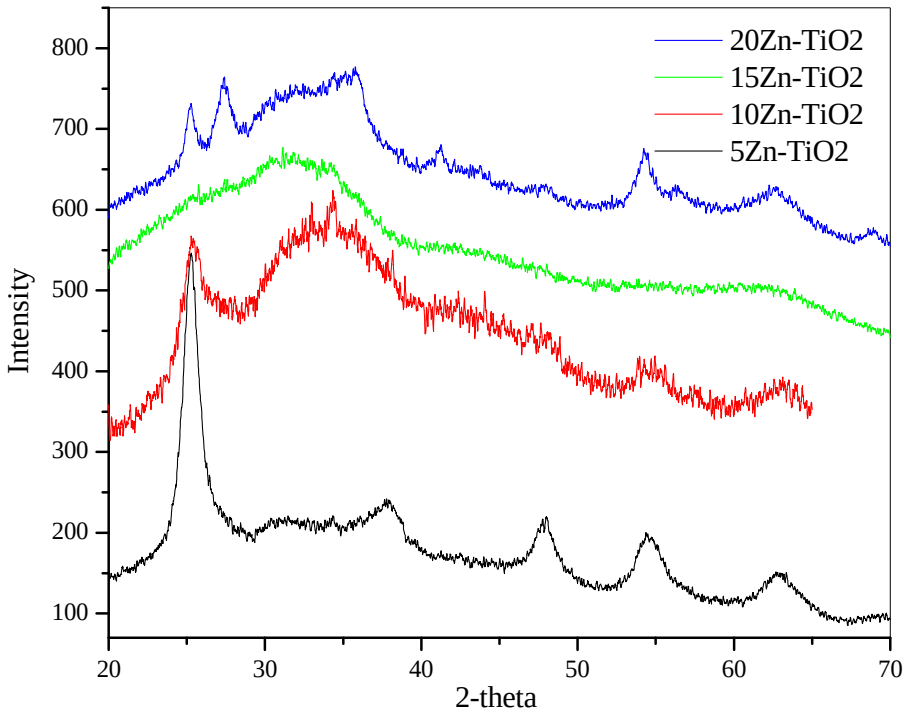

Fig. 3. X-ray diffraction patterns for Zn-TiO_2 catalysts with 5-20%Zn loading.

The XRD patterns of 10%Co-TiO_2, 10%Zn-TiO_2, 10%Ni-TiO_2, and 10%Sn-TiO_2 samples showed no peaks that can be attributed to the metal or metal oxides. This could be due to one or more reasons which include the non-crystalline nature of particles, highly uniform

dispersion,preferential orientation of particles and very small sizes making themX-ray-amorphous.**Fig.3** shows the XRD spectra of Zn-TiO_2 catalyst samples illustrating the crystallization behavior of $TiO_2$with Zn loading varying from 5-20%. As observed with other metals, the addition of Zn to TiO_2 matrix resulted in decreased peak intensities, owing to the lower crystallinity of TiO_2.It clearly indicates that the presence of metal atoms hinder or delays the TiO_2 crystallization process, which was corroborated by the TGA-DSC studies.

The rate of crystallization during heat treatment depends on the rate of atomic diffusivity of titanium ions. However, the presence of metal atoms could be acting as an impurity or adatoms decreasing the mobility of Ti ions resulting in decreased diffusivity and subsequent decreased crystallization[26, 27]. The sizes of TiO_2, CuO and PdOcrystallites determined using Scherrer equation are shown in **Table 1**.The decreased sizes of TiO_2 crystals upon metal loading further confirmed the lower crystallinity.For instance, the average TiO_2 crystallites size of ~17.2 nm decreased by more than 50% to ~4-9.8 nm upon metal addition. The extent of decreased crystallinity was also observed to be dependent on the metal type and loading.

3.3. N_2-Physisorption Analysis to Study Textural Properties of M-TiO_2

The N_2 adsorption-desorption isotherms for TiO_2 and different M-TiO_2samples with 10%metal loading are depicted in **Fig.4(A)**. All isotherms resembled the Type IV isotherm,a typical characteristic for mesoporous materials, based on IUPAC classification[28].

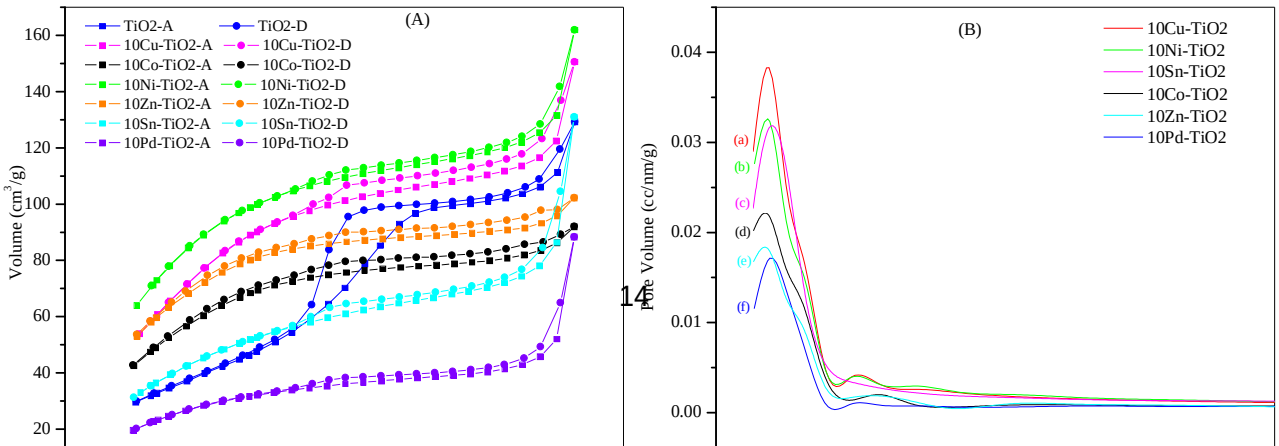

Fig. 4. (A) N_2 adsorption-desorption isotherms, and (B) BJH pore size distributionfor different M-TiO_2 catalyst samples.

The hysteresis loop associated with isotherms is attributed to the capillary condensation which also confirms the presence of mesoporous structure. While TiO_2isotherm showed a H2 type hysteresis loopcorresponding to the inkbottle shaped pores, the shape of the hysteresis loop changed from H2 to H4 upon incorporationof metal particles,indicating a significant change in the textural properties. The H4 type hysteresis loops generally correspond to the slit-like pores.Asharp rise in N_2 uptake at relative pressure above 0.95 is due to the N_2 condensation ininter-particle pores.**Figure 4(b)** depicts the BJH pore size distribution of different M-TiO_2 catalysts indicating reasonably narrow distribution in the range of 3 to 4 nm. **Table 1** summarizes the BET surface areas, pore sizes, and pore volumes of the different M-TiO_2catalyst samples investigated in this study.TiO_2 showed a high surface area of 146.6 m^2/g, pore size of 4.7 nm and pore volume of 0.17 cm^3/g. However, depending on the type of metal incorporated in TiO_2, the surface area, pore diameter, and pore volume varied significantly in the range of 99.7-309.8 m^2/g, 2.53-4.93nm, and 0.08-2.03cm^3/g, respectively, indicating a strong influence of the metal ions on TiO_2 textural properties.For instance, whilethe incorporation of Pd in TiO_2significantlydecreased the surface area by about 32%, the addition of Coremarkablyincreased it by about 111% to 309.8 m^2/g.

The increase in surface area of M-TiO_2 samples with the addition of metalsis similar to that reported by Youn et al.[29]who observed that the addition of small quantity ofmetal ions promoted the textural stability of mesoporous ZrO_2 resulting in an increased surface area. However, the underlying reasons were not discussed in detail.We believe that the effect of metal incorporation on the textural properties of mesoporous TiO_2 is linked to the influence of metal ions on the crystallization behavior of TiO_2that was also observed in the TGA-DSC and XRD studiesdescribed in previous sections. Crystallization of mesoporousTiO_2 upon calcination leads to the loss of the mesoporous structure due to the increased crystallite sizes, thus decreasing the surface area[27]. The degree of decreasedsurface area depends upon the degree of crystallization.Thus, the higher surface area of M-TiO_2 compared to TiO_2 can be attributed to relatively lower extent of crystallization upon metal addition.However, this effect was not observed in 10%Pd-TiO_2 sample, where the specific surface area decreased uponaddition of Pdcompared to TiO_2 itself.The observed contradictory influence of Pd compared to other metals on M-TiO_2 surface area can be explained on the basis of its crystal sizes. The significantly larger Pd crystal sizes of about 49.4 nm (**Table 1**) could be responsible for the collapse of TiO_2 mesoporous structure leading to a reduction in surface area.

The textural properties of Zn-TiO_2 catalyst samples with different metal loadings of 5-20% are also presented in **Table 1**. An interesting behavior was observed in surface area variation when the Zn loading was increased from 0 to 20%. The surface area increased from ~146 to ~257.5 m^2/g with the increase in Zn loading from 0 to 15%. However, further increase in Zn loading to 20% resulted in a drastic reduction in surface area to 140.1 m^2/g.The first trend in surface area variation can be explained on the basis of delay in crystallization of TiO_2due to the presence of Zn atoms,as discussed above and evident in TGA-DSC results (**Fig. 1b**). The Zn

atoms hinder the crystallization of TiO_2avoiding the collapse of mesoporous structure up to 15% loading. However, when the Zn loading is increased to 20%, Zn atoms could be interferingwith the formation of mesoporous structure itself. Thus, the observed lower surface area for 20%Zn-TiO_2 compared to TiO_2can be attributed to the lack of mesoporous structure.

3.4. Chemical Composition Analysis using ICP-OES

The metal loadings in M-TiO_2 samples, determined using ICP-OES analysis, are shown in **Table 1**. Themetal loadingsvaried in the range of 10.6 to 13.9%except for samples of 10%Sn-TiO_2 and 10%Pd-TiO_2. For Sn and Pd catalysts, the loading was found to be considerably lower (5.26 and 5.32%) than the intended loading of 10%. While, the higher loading of metal can be attributed to the more loss of titania particles or precursor, the lower metal loading in some cases could be due to the loss of metal particles or precursors during the catalysts preparation.

3.5. FTIR Analysis

Fig.5a and b show the FTIR spectra of typical as-prepared and calcined samples of TiO_2 and 10%Zn-TiO_2, respectively.

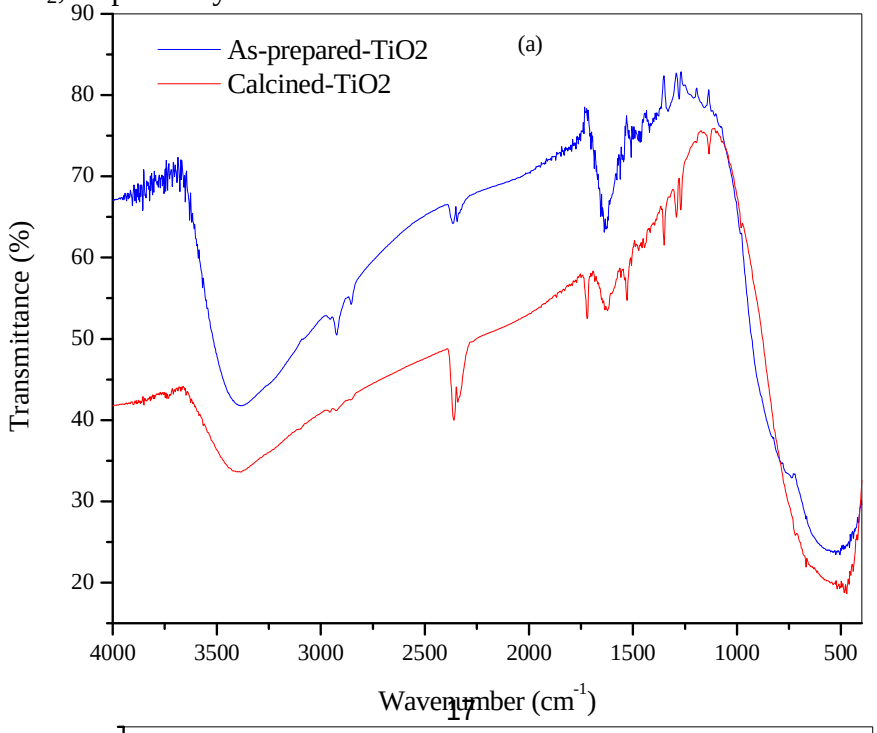

Fig 5. FTIR spectra of as-prepared and calcined samples of: (a) TiO_2 and (b) 10%Zn-TiO_2.

A doublet band centered at ~2920 cm^{-1} and ~2854 cm^{-1} observed in both as-prepared samples and a broad high intensity band at about 1470 cm^{-1} in 10%Zn-TiO_2 sample (this band seems to be overlapped in wide band between 1520-1720 cm^{-1} for TiO_2 sample) corresponds to the symmetric -CH and asymmetric -CH_2 vibrations of the organic template, CTAB, that disappeared upon calcination confirming its complete removal by combustion[30]. The strong band in the range of 900-400 cm^{-1} is associated with vibration modes of Ti-O in TiO_2[31].While, the broad adsorption bands in the range of 3800 – 3000 cm^{-1} are assigned to the stretching vibrations of -OHfrom physisorbed water molecules, the adsorption band around ~1630 $cm^{-1}$is ascribed to the -OH bending vibrations arising from coordinated water on support surface [32]. The adsorption bands ~2350 cm^{-1} correspond to atmospheric CO_2.

3.6. Microscopic Analysis of M-TiO_2 catalysts

Fig. 6 shows therepresentative TEM images of the calcined TiO_2 and M-TiO_2samples. **Fig.6(a-c)** clearly show that both TiO_2 and M-TiO_2 have disordered but highly mesoporous structure indicating that the porous structure is intact after incorporation of 10% metal in one-step synthesisprocedure. The sizes of the pores ranged between 2.5 nm to 5 nm confirming the results of N_2-physisorption studies. The dark spots in the high contrast TEM image shown in **Fig.6d** indicate the uniform distribution of the cobalt particles in TiO_2 matrix.The SEM images of different calcined M-TiO_2 catalysts with metal mapping acquired using EDX analysis are shown in **Fig.7**. The sizes of the bulk catalyst particles varied in the range of 2-40 µm. Thesignificant differences in the dispersion of different metals in TiO_2 support are clearly evident from visual inspections. The highest dispersion was observed for 10%Co-TiO_2 which was followed by 10%Pd-TiO_2.While Ni-TiO_2 and Sn-TiO_2 showed similar but relatively moderate dispersion, the least dispersion was noticed in Zn-TiO_2 and Cu-TiO_2 samples. The clarification of these observations is further bolstered by TPR resultsdiscussed in the following section.

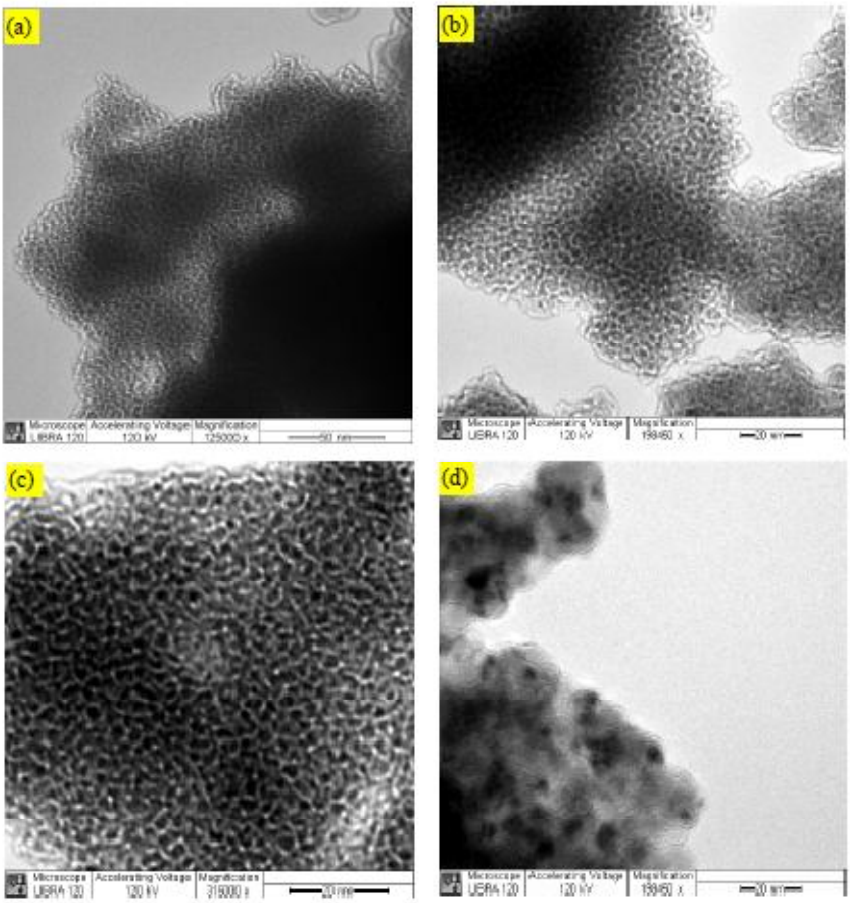

411

412

413 **Fig. 6:** TEM images of (a) TiO_2 (b) 10%Sn-TiO_2 (c) 10%Zn-TiO_2 and (d) 10%Co-TiO_2.

414

415

416

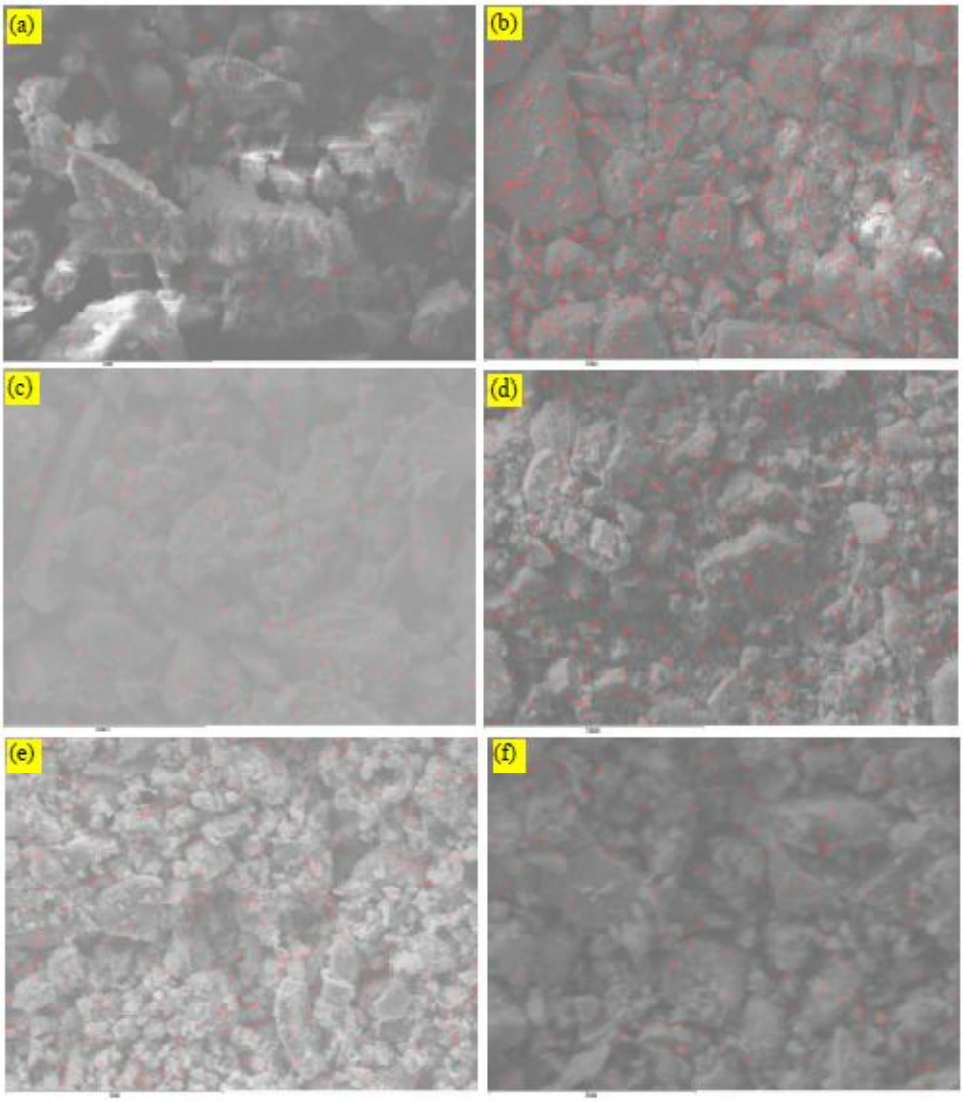

Fig. 7. SEM images with EDX elemental mapping for (a) 10%Cu-TiO_2 (b) 10%Co-TiO_2 (c) 10%Ni-TiO_2 (d) 10%Pd-TiO_2 (e) 10%Sn-TiO_2 and (f) 10%Zn-TiO_2

3.7. Effect of Metal-Support Interactionon Reduction Behavior of M-TiO_2Catalysts

TiO_2 is known to interact with supported metal components affecting the catalyst's properties and subsequently its catalytic performance. Therefore, H_2-TPRstudiesof M-TiO_2 catalysts can provide information on the interactions between the metal and TiO_2 support[33],

which can be correlated to its catalytic activity for methanol steam reforming reactions.**Fig.8** shows a series of TPR profiles for different M-TiO_2 catalyst samples carried out under identical operating conditions, illustrating the reduction behavior of incorporated metal oxides.The TPR profile of TiO_2(**Fig. 8a**) showed a broad low intensity peak in the temperature range of 410-630°C, indicating the reduction of surface TiO_2 molecules. Other researchers have also foundsimilar TiO_2reduction behavior, withthe observed reduction temperature varied between 400 and 720 °C [34-37].

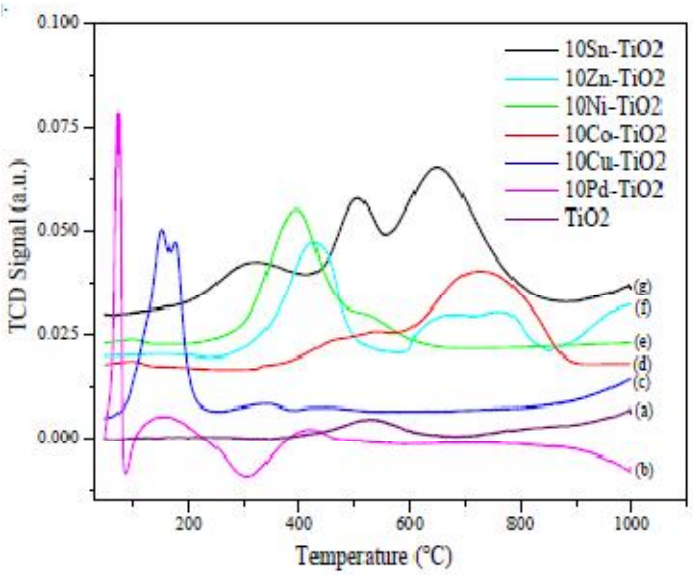

Fig. 8. TPR profiles of different M-TiO_2 catalyst samples.

The TPR profile of 10%Pd-TiO_2shown in **Fig. 8b**exhibited an interesting reduction behavior. The consumption of H_2 started at 50 °C and yieldedanintense peak centered at 73 °Cthat corresponds to reduction of PdO on the surface to Pd^0[38, 39].With further increase in temperature, four more peaks were observed:a sharp negative peak (81-108 °C), a wide positive peak (105-225 °C), a wide negative peak (225-383 °C) and a low intensity positive peak (383-460 °C). The positive peak centered at about 160 °C corresponds to the reduction of PdO particles located inside the porous structure which are more dispersed due to the comparatively

stronger interactions with TiO_2 support[10, 40, 41]. Both PdO reduction peaks were followed by negative peaks which can be attributed to the release of H_2 from the decomposition of the palladium hydride (PdH). The observedPdH decomposition at about 85 °C is in good agreement with earlier reports [40, 42]; however, the peak observed at higher temperature of about 300 °C was not reported before. We believe that Pd^0 formed at both stages of reduction undergoes the hydride formation which subsequently decomposedwith increase in temperature resultingin negative peaks. Finally, the peak centered at 420 °C is assigned to the reduction of TiO_2 surface molecules. The observed decrease in the reduction temperature of TiO_2 from 530 °C to 420 °C in the presence of Pd is attributed to the interactions between Pd and TiO_2 which have also been observed for other noble metals [36, 43]. Shen et al.[38]suggested that the dissociationof hydrogen on the Pd particles and its successive spillover to TiO_2 leads to its lower temperature of reduction. These moderate to higher levels of interactions between Pdand TiO_2 surface could be responsible for the observed uniform dispersion of Pd in TiO_2 as shown in EDX studies (**Fig.7d)**.The TPR profile of 10%Cu-TiO_2(**Fig. 8c**) showed two overlapping peaksof high intensity in the temperature range of 60-250 °C.They were followed by a wide and very low intensity peak spanned between 260 to 380 °C. Similar reduction behavior with coinciding peaks was also observed by other researchers[44, 45].These peaks indicated theco-existence of three types of copper species in the calcined 10%Cu-TiO_2 sample. While the first two peaks centered at 153°Cand 175 °Cwere attributed to the reduction of bulk CuO species with comparatively insignificant but varying degree of interactions, the third peak suggested the reduction of bulk crystalline copper oxidethathas moderate interactions with TiO_2 support [46-48].The TPR profile also showed a very low intensity peak in the temperature range of 400-500 °C that can be attributed to the reduction of surface TiO_2.Larsson et al. observed a significant decrease in the

reduction temperature of TiO_2 in the presence of CuO,suggesting an interaction between CuO and TiO_2[49, 50].Thus, the observation of very low peak intensity with a small shift in reduction temperature could be due to insignificant interactions between CuO and TiO_2 in the present study. This is consistent with the EDX mapping of Cu shown in **Fig.7a** where copper was seen to be poorly dispersed compared to the other metals.

The TPR profile of 10%Co-TiO_2 contained a broad area of H_2 consumption which started at 320 °C and continued to about 900 °C.The broad peak area apparently consisting of several overlapping reduction peaks can be de-convoluted into three peaks with first centered at 460 °C, second at 535 °C and last one at 720 °C. The overlapping behavior of first and second peak was in good agreement with other studies which were assigned to the stepwise reduction of Co_3O_4 to metallic Co (Co^{3+} ===> Co^{2+} ===> Co^0) [51-53]. By analogy to previous studies,the major peak observed at 720 °C can be attributed to the reduction of cobalt titanate ($CoTiO_3$)[54, 55].However, it should be noted that although the behavior of the reduction was consistent with some of the earlier studies, the reduction peak positions in the present study are observed at comparatively higher temperature[56-59]. While Jalama et al. [57] observed the three analogous peaks at 344, 373 and 545 °C, Riva et al. found them in the range of 300 to 720 °C [56]. Thus, based on the TPR data and high dispersion of Co in the TiO_2 matrixobserved in EDX analysis (**Fig.7b)** it can be inferred that very strong interactions exist between cobalt and TiO_2 support in the 10%Co-TiO_2 catalyst synthesized in this study using one-step method.

In contrast to the high temperature reduction behavior of Co-TiO_2, complete reduction of 10%Ni-TiO_2catalyst sample was achieved by 600 °C. The main sharp peak at 400°C was followed by a low intensity wide shoulder peak centered at ~530 °C. While the first peak can be assigned to the reduction of NiO particles having moderate interaction with the TiO_2 surface, the

second peak is attributed to the reduction of NiO having moderate-to-stronger interactions with TiO_2[14, 60].In general, the reduction of bulk NiOparticles in the absence of interactions with the support occurs in the temperature range of 280-300°C[61, 62]. The nonexistenceof this peak indicates that the present 10%Ni-TiO_2catalyst prepared by one-pot synthesis method does not contain such bulk NiO particles. Furthermore, H_2 consumption peaks for the reduction of $NiTiO_3$,which are generally observed above 600 °C are not present suggesting the absenceof very strong NiO-TiO_2interactions[60, 63]. Yan et al. [60] claimed that both these bulk NiO and $NiTiO_3$ are catalytically inactive and interestingly they are not present in our 10%Ni-TiO_2 catalyst.The observed moderate interactions between Ni and TiO_2 were also evident in the reasonable dispersion of Ni shown in **Fig.7c** of EDX studies.

The H_2 consumption profile as a function of temperature for 10%Zn-TiO_2 catalyst sample is presented in **Fig.8f**.The TPR profile shows one clearsymmetric peak at about430°C and two overlapping peaks centered at about 650 °C and 750 °C. Itis interesting to note that a significant portion of ZnO in TiO_2 was reduced well below the generally reported bulk ZnOreduction temperature of about 650 °C [64, 65].This clearly indicatesthe existence of the strong-metal support interactions between Zn and TiO_2 promoting the reduction of ZnO. The presence of reduction peak at 750 °C can be attributedto the very strong metal-support interaction leading to the formation of Zn-titanate spinel structures. Finally, the TPR profile for 10%Sn-TiO_2(**Fig. 8g**) shows three distinct overlapping reduction peaksin the temperature range of150-800°C. Nava et al.[66] and Corradini et al.[67] also reported similar three stage reduction behavior for Sn/TiO_2.The H_2 consumption peak at 320 °C is assigned to the reduction of SnO_2 species which are strongly interacting with the TiO_2 surface. The two other peaks centered at 500 °C and 650 °C are attributed to the two step reduction ofbulk SnO_2 to metallic Sn(Sn^{4+}===> Sn^{2+}===>Sn^0)

[68].As the reported temperature for bulk SnO_2reduction is generally above 750 °C [69], the observed lower reduction temperature of bulk SnO_2 in the present study shows the existence of varied degree of interactions between the Snparticles and TiO_2.

3.8. Performance test of M-TiO_2 for SRM

To gain further insights in to the metal-support interactions, the comparative performance of different metal componentsincluding Cu, Co, Ni, Pd, Zn and Sn incorporated in mesoporous TiO_2 support was investigated for H_2 production.**Fig. 9**illustrates the catalytic behavior of each catalyst for SRM showing the effect of reaction temperature on methanol conversion and selectivity towards different products, namely, H_2, CO, CO_2 and CH_4. One common trend observed was the increase in methanol conversion with increase in reaction temperature for all catalysts showing a strong influence of temperature on the catalysts' activity. For example, for 10%Pd-TiO_2 catalyst, methanol conversion increased from 8% to about 98 % with increase in temperature from 150 °C to 350 °C. This can obviously beattributed to the endothermic nature of steam reforming reaction (**Eq.(5)**).

$$CH_3OH + H_2O \leftrightarrow CO_2 + 3H_2 \qquad \Delta H° = 90.6\ kJ/mol \qquad (5)$$

$$CH_3OH \leftrightarrow CO + 3H_2 \qquad \Delta H° = 49.5\ kJ/mol \qquad (6)$$

$$CO + H_2O \leftrightarrow CO_2 + H_2 \qquad \Delta H° = -41.1\ kJ/mol \qquad (7)$$

$$CO + 3H_2 \leftrightarrow CH_4 + H_2O \qquad \Delta H° = -206\ kJ/mol \qquad (8)$$

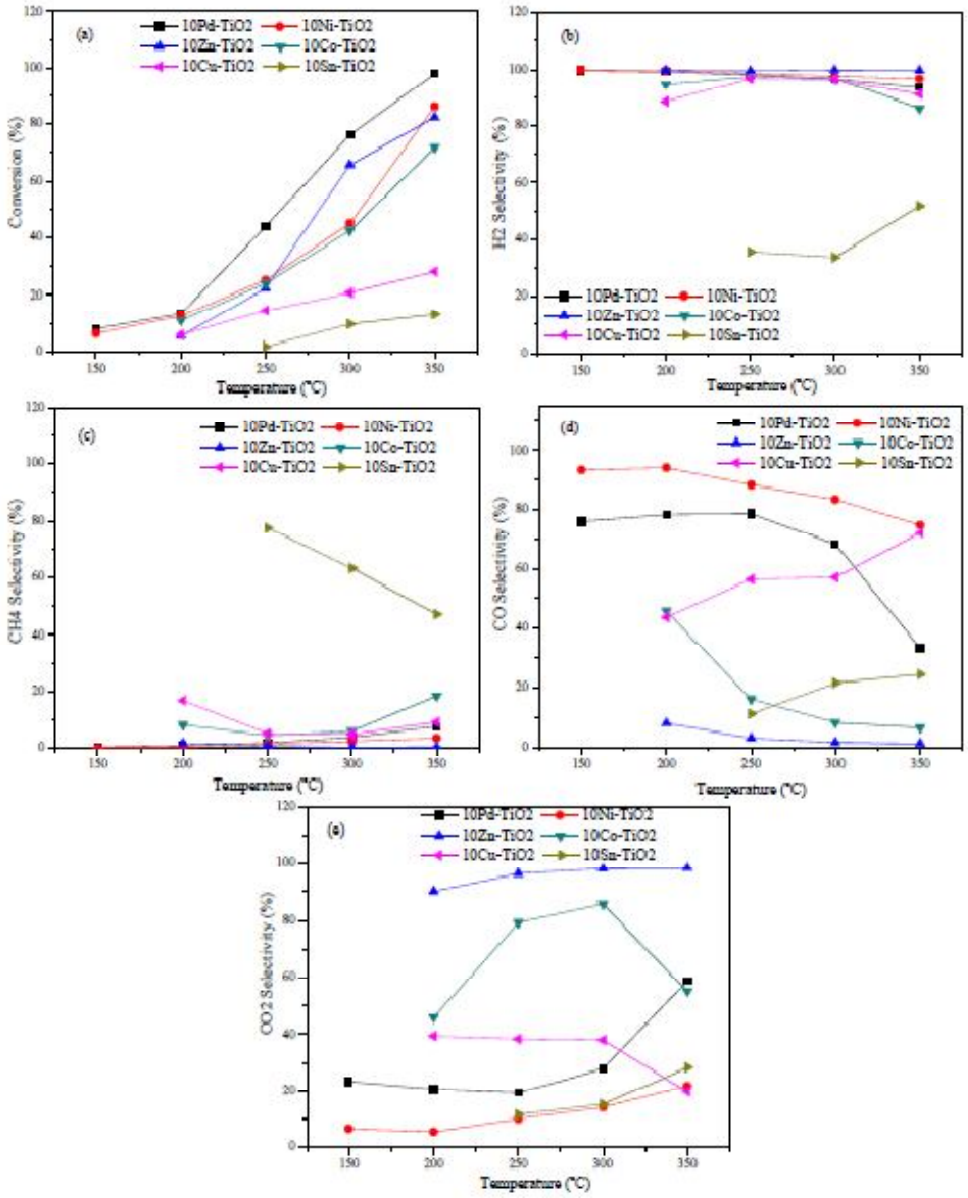

Fig. 9. The effect of reaction temperature on: (a) methanol conversion (b) H_2 selectivity (c) CH_4 selectivity (d) CO selectivity (e) CO_2 selectivity for different M-TiO_2 catalysts

The conspicuous outcome of these results (**Fig. 9**) is the remarkable differences in the SRM activity and selectivity among the different metal componentsincorporated in TiO_2. The methanol conversion vs temperature profiles in **Fig. 9a**reveal that whilePd/TiO_2 catalyst isthe most active, Sn/TiO_2isthe least activefor SRM reaction establishing an overall activity trendofPd> Ni > Zn > Co >> Cu >> Sn. This activity sequence of M-TiO_2can be linked to the

specific interactions observed between the metal component and the TiO_2 support (TPR section, above). The ease of PdO reduction and moderate to stronger interactions between Pd and TiO_2 resulting in higher dispersioncould be responsible for its observed highest activity. In contrast, very strong metal-support interactions observedin 10%Co-TiO_2led to high dispersion of Co,theconsequential high temperature reduction could be responsiblefor its lower SRM activity. For both Ni and Zn where the specific metal-support interactions led to lower reduction temperature compared to their bulk counterparts, reasonable SRM activity next to Pd was observed. For example, at 350 °C, 10%Ni-TiO_2 and 10%Zn-TiO_2yielded about 86% and 82% methanol conversion, respectively. The significantly lower activity of 10%Cu-TiO_2catalyst could be ascribed to the absence of noticeable metal-support interactions resulting in lower dispersion and sintering.In contrast, in our very recent study[70],Cu-MCM-41 showed excellent activity and selectivity for SRM. Given the inert nature of silica support reducing or eliminating the possible metal-support interactions, the outstanding performance of Cu-MCM-41 was attributed to highly uniform dispersion of Cu in very high surface area MCM-41 support. The resultsfor Ni-TiO_2 and Cu-TiO_2catalysts in this studyare similar to that observed for ethanol steam reforming activity of Ni/γ-Al_2O_3 and Cu/γ-Al_2O_3catalysts reported by Aupretre et al. [71]. However, in their studies, Zn/γ-Al_2O_3 showed significantly lower activity compared to Ni/γ-Al_2O_3. The higher SRM activity of Zn-TiO_2which was comparable to that of Ni-TiO_2in the present studysupportsour hypothesisthat thespecific interactions between Zn and TiO_2observed in TPR analysis are responsible for its promising SRM activity.Interestingly, even though moderate level of interactions were observed between Sn and TiO_2 resulting in a portion of SnO_2reduction at lower temperature, it showed an insignificant activity for SRM reaction with just 10% conversion at 350 °C.These results further suggest thatfor favorable steam reforming activity, there need to

562 exist optimum interactions between support and metal components which are again
563 characteristics of the particular metal-support system.

564 While methanol conversion varied significantly for different M-TiO_2 catalysts, all of
565 themshowed more than 90% H_2 selectivity exceptforSn-TiO_2,where the selectivity dropped to
566 less than 50% due to excessive methanation reaction (**Eq.(8)**)as shown in **Fig. 9**.It wasobserved
567 that although both Ni-TiO_2 and Pd-TiO_2 exhibited very good activity for decomposition reaction
568 leading to higher methanol conversions (**Eq.(6)**), the activity for water-gas-shift reaction (**Eq.(7)**)
569 was almost insignificant resulting in very high (>80% for Ni and >70% for Pd at 350) CO
570 selectivitiesover the range of reaction temperature shown in **Fig. 9d**. The selectivity of CO was
571 also observed to depend on the relative activity for the water-gas-shift reaction(**Eq.(7)**) and
572 methanation reaction(**Eq.(8)**). Although methanation reaction does help in decreasing CO
573 selectivity, one mole CH_4 formation results in loss of 3 moles of product H_2.For
574 example,comparatively lower CO selectivity observed for Co-TiO_2, Cu-$TiO_2$and Sn-TiO_2were
575 attributed to the formation of methane at the expense of decreased H_2 selectivity.On the other
576 hand, Zn-TiO_2 showed the best performance among the studied catalysts both in terms of desired
577 higher activity for water-gas-shift and lower activity formethanation reaction. Based on
578 theimportant criterion of lower CO selectivity, the different metals followed the order: Zn-TiO_2<
579 Sn-TiO_2< Co-TiO_2< Cu-TiO_2< Pd-TiO_2< Ni-TiO_2.

580 As Zn-TiO_2 catalyst exhibited lowest CO selectivity among different metals studied, Zn loading
581 was varied from 5-20% to investigate further the effect of Zn loading on SRM activity and
582 selectivity.The results of these SRM studies are presented in **Fig. 10.**It was interesting to note
583 that the SRM activity increased with increase in loading up to 15% and then decreased with
584 further increase in Zn loading. For example, at 300 °C reaction temperature, the conversion

increased from 28% to 66% with increase in Zn loading from 5% to 10%. It remained almost constant at 15% loading giving slightly higher conversion of ~68%. However, further increase in Zn loading to 20% drastically decreased methanol conversion to only about 19%.

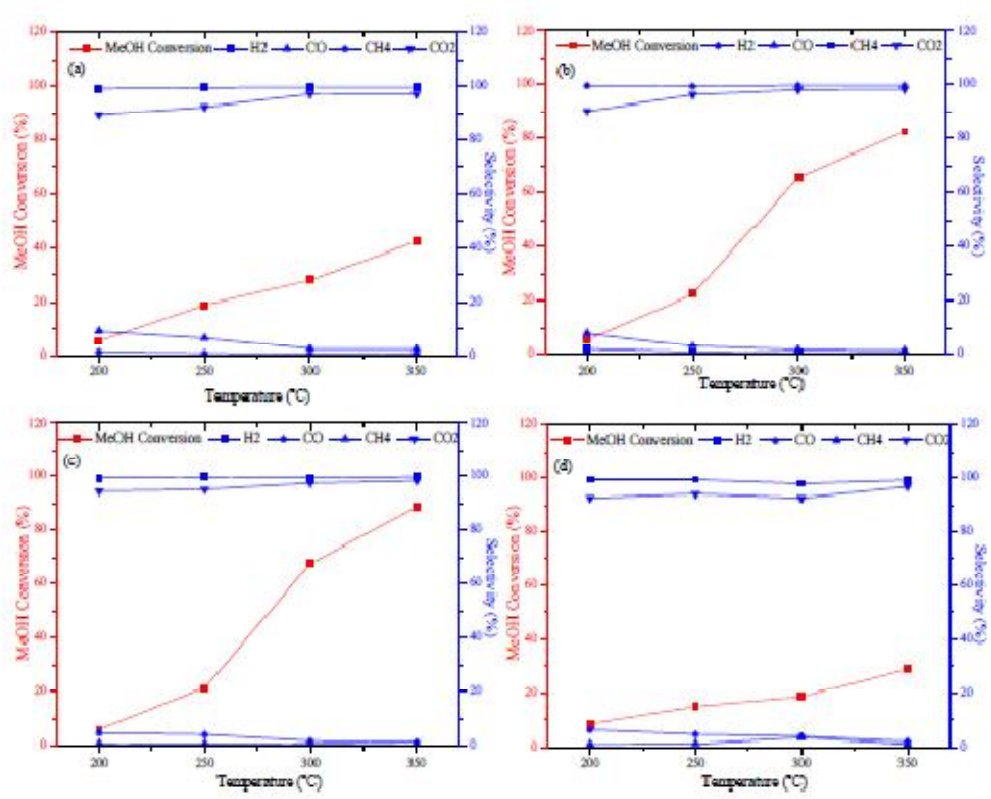

Fig. 10. The effect of reaction temperature on methanol conversion and product selectivity for (a) 5%Zn-TiO_2 (b) 10%Zn-TiO_2 (c) 15%Zn-TiO_2 and (d) 20%Zn-TiO_2 catalysts.

This behavior is consistent with observed variations in surface area ofZn-TiO_2 catalyst with changes in Zn loading (**Table 1**). The surface area of Zn-TiO_2 catalyst was also observed to increase with increase in Zn loading from 5 to 15% and then decreased drastically at 20% Zn loading. Thus, the observed change in the SRM activity with Zn loading can be attributed to its influence on the catalyst surface area. The observed methanol conversion and CO selectivity values indicate that the 15%Zn-TiO_2 is the most favorable catalyst among the different catalysts investigated in the present investigation.

4. Conclusions

A simple one-step procedure was used to synthesize different mesoporous M-TiO_2 (M: Cu, Co, Ni, Pd, Sn, and Zn) catalysts for investigatingthe specific metal-TiO_2interactions and their influence on SRM activity and selectivity.Synthesized M-TiO_2 catalysts showed significantly high surface areas in the range of 99-309 m^2/g depending on the type of incorporated metal species. TGA-DSCand XRD studies revealed thatincorporation of metal ions significantly delayed the TiO_2 crystallization which can be attributed to the decreased mobility of Ti ions caused by metal atoms acting as impurity or adatoms.This delayed crystallization led to the formation of M-TiO_2 catalysts with significantly higher surface areas compared to TiO_2itself. Both the type of metal and loading significantly influenced the textural properties of prepared catalysts. The results from SRM studies indicatedthe remarkable differences in catalytic performances of different M-TiO_2 catalystsdue to specific metal-support interactions controlling the reducibility and dispersion of metal particles in TiO_2 matrix.While the SRM activity for different M-TiO_2 catalysts followed the sequence of Pd-TiO_2> Ni-TiO_2> Zn-TiO_2> Co-TiO_2>> Cu-TiO_2>> Sn-TiO_2, the lower CO selectivity was observed in the order of Zn-TiO_2< Sn-TiO_2< Co-TiO_2< Cu-TiO_2< Pd-TiO_2< Ni-TiO_2. Furthermore, the SRM activity of Zn-TiO_2catalysts was observed to increase with increase in Zn loading from 5 to 15% and then decreased with further increase in Zn loading to 20%. The observed optima for Zn-TiO_2 catalyst with variation in Zn loading was attributed to its substantial influence on the textural properties. Among the different catalysts investigated in the present study, 15%Zn-TiO_2 showed best SRM performance with 88% methanol conversion, ~100% H_2 selectivity and 1.3% CO selectivity at 350 °C reaction temperature.

Acknowledgement

622 The authors acknowledge the funding received from National Science Foundation (NSF) for the
623 NSF-CREST Bioenergy Center (Grant No. HRD-124215). The authors would like to thank Dr.
624 Shamsuddin Ilias for the use of his BET set-up for surface analysisand Dr. Lijun Wang for use of
625 his Chemical Analyzer for TPR studies. The authors are also grateful to Mr. James King
626 (Chemistry Department) for his support in the experimental work, Mr. Bryce Holmes (School of
627 Agriculture and Environmental Sciences) for his help with ICP analysis.The authors thank Dr.
628 Jag Sankar and Dr. Sergey Yarmolenko (Center for Advanced Materials and Smart Structures-
629 CAMSS) at NCAT for the use of the XRD for material characterization. Finally, we
630 acknowledge the Joint School of Nanoscience and Nanoengineering (JSNN) for using the TEM
631 and SEM-EDX instruments.

References

[1] US-DOE, Department of Energy, Washington, DC, USA, 2013.

[2] J.S. Spendelow, D.C. Papageorgopoulos, Fuel Cells. 11 (2011) 775-786.

[3] F. de Bruijn, Green Chemistry. 7 (2005) 132-150.

[4] M.A.J. Cropper, S. Geiger, D.M. Jollie, J. Power Sources. 131 (2004) 57-61.

[5] A. Faur Ghenciu, Curr. Opin. Solid State Mater. Sci. 6 (2002) 389-399.

[6] M. Krumpelt, T.R. Krause, J.D. Carter, J.P. Kopasz, S. Ahmed, Catal. Today. 77 (2002) 3-16.

[7] A. Bshish, Z. Yaakob, B. Narayanan, R. Ramakrishnan, A. Ebshish, Chem. Pap. 65 (2011) 251-266.

[8] J.M. Silva, M.A. Soria, L.M. Madeira, Renewable and Sustainable Energy Reviews. 42 (2015) 1187-1213.

[9] R. Pérez-Hernández, D. Mendoza-Anaya, A.G. Martínez, A. Gómez-Cortés, Hydrogen Energy- Challenges and Perspectives, 2012.

[10] H. Tidahy, S. Siffert, J.-F. Lamonier, E. Zhilinskaya, A. Aboukaïs, Z.-Y. Yuan, A. Vantomme, B.-L. Su, X. Canet, G. De Weireld, Appl. Catal. A: Gen. 310 (2006) 61-69.

[11] M. Vannice, R. Garten, J. Catal. 56 (1979) 236-248.

[12] C.H. Bartholomew, R.B. Pannell, J.L. Butler, J. Catal. 65 (1980) 335-347.

[13] F. Pinzari, P. Patrono, U. Costantino, Catal. Commun. 7 (2006) 696-700.

[14] V. Nichele, M. Signoretto, F. Menegazzo, I. Rossetti, G. Cruciani, Int. J. Hydrogen Energy. 39 (2014) 4252-4258.

[15] I. Rossetti, J. Lasso, E. Finocchio, G. Ramis, V. Nichele, M. Signoretto, A. Di Michele, Appl. Catal. A: Gen. 477 (2014) 42-53.

[16] A. Gribovskii, L. Makarshin, D. Andreev, S. Korotaev, P. Dutov, R. Khantakov, S. Reshetnikov, V. Parmon, Kinet. Catal. 50 (2009) 11-17.

[17] J. Rasko, A. Hancz, A. Erdőhelyi, Appl. Catal. A: Gen. 269 (2004) 13-25.

[18] G. Martra, Appl. Catal. A: Gen. 200 (2000) 275-285.

[19] J. Chen, N. Yao, R. Wang, J. Zhang, Chem. Eng. J. 148 (2009) 164-172.

[20] P.D. Vaidya, A.E. Rodrigues, Chem. Eng. J. 117 (2006) 39-49.

[21] B. Zhang, X. Tang, Y. Li, W. Cai, Y. Xu, W. Shen, Catal. Commun. 7 (2006) 367-372.

[22] X. Hu, G. Lu, Appl. Catal. B: Environ. 99 (2010) 289-297.

663 [23] E.P. Barrett, L.G. Joyner, P.P. Halenda, J. Am. Chem. Soc. 73 (1951) 373-380.
664 [24] M. Arsalanfar, A. Mirzaei, H. Bozorgzadeh, H. Atashi, S. Shahriari, A. Pourdolat,
665 Journal of Natural Gas Science and Engineering. 9 (2012) 119-129.
666 [25] V.G. Deshmane, Y.G. Adewuyi, Microporous Mesoporous Mater. 148 (2012) 88-100.
667 [26] P. Mercera, J. Van Ommen, E. Doesburg, A. Burggraaf, J. Ross, Applied catalysis. 57
668 (1990) 127-148.
669 [27] P. Mercera, J. Van Ommen, E. Doesburg, A. Burggraaf, J. Roes, Applied catalysis. 78
670 (1991) 79-96.
671 [28] K. Sing, D. Everett, R. Haul, L. Moscou, R. Pierotti, J. Rouquerol, T. Siemieniewsks,
672 Pure Appl. Chem. 57 (1985) 603-619.
673 [29] M.H. Youn, J.G. Seo, I.K. Song, Int. J. Hydrogen Energy. 35 (2010) 3490-3498.
674 [30] V.G. Deshmane, Y.G. Adewuyi, Fuel. 107 (2013) 474-482.
675 [31] D. Huang, Y. Wang, L. Yang, G. Luo, Microporous Mesoporous Mater. 96 (2006) 301-
676 306.
677 [32] V.G. Deshmane, Y.G. Adewuyi, Appl. Catal. A: Gen. 462–463 (2013) 196-206.
678 [33] N.W. Hurst, S.J. Gentry, A. Jones, B.D. McNicol, Catal. Rev. Sci. Eng. 24 (1982) 233-
679 309.
680 [34] H. Zhu, Z. Qin, W. Shan, W. Shen, J. Wang, J. Catal. 225 (2004) 267-277.
681 [35] K.-R. Hwang, S.-K. Ihm, S.-C. Park, J.-S. Park, Int. J. Hydrogen Energy. 38 (2013) 6044-
682 6051.
683 [36] J. Peng, S. Wang, Appl. Catal. B: Environ. 73 (2007) 282-291.
684 [37] J. Wang, A. Cuan, J. Salmones, N. Nava, S. Castillo, M. Moran-Pineda, F. Rojas, Appl.
685 Surf. Sci. 230 (2004) 94-105.
686 [38] W.-J. Shen, M. Okumura, Y. Matsumura, M. Haruta, Appl. Catal. A: Gen. 213 (2001)
687 225-232.
688 [39] I. Eswaramoorthi, A.K. Dalai, Int. J. Hydrogen Energy. 34 (2009) 2580-2590.
689 [40] M. Hosseini, S. Siffert, H. Tidahy, R. Cousin, J.-F. Lamonier, A. Aboukais, A.
690 Vantomme, M. Roussel, B.-L. Su, Catal. Today. 122 (2007) 391-396.
691 [41] R. Pérez-Hernández, A. Avendaño, E. Rubio, V. Rodríguez-Lugo, Top. Catal. 54 (2011)
692 572-578.

693 [42] C.-B. Wang, H.-G. Lee, T.-F. Yeh, S.-N. Hsu, K.-S. Chu, Thermochim. Acta. 401 (2003)
694 209-216.
695 [43] H. Liang, Y. Zhang, Y. Liu, Journal of Natural Gas Chemistry. 17 (2008) 403-408.
696 [44] P.M. Sreekanth, P.G. Smirniotis, Catal. Lett. 122 (2008) 37-42.
697 [45] X.-F. Yu, N.-Z. Wu, Y.-C. Xie, Y.-Q. Tang, J. Mater. Chem. 10 (2000) 1629-1634.
698 [46] F. Coloma, F. Marquez, C.H. Rochester, J.A. Anderson, PCCP. 2 (2000) 5320-5327.
699 [47] J. Xiaoyuan, D. Guanghui, L. Liping, C. Yingxu, Z. Xiaoming, J. Mol. Catal. A: Chem.
700 218 (2004) 187-195.
701 [48] C.-S. Chen, J.-H. You, J.-H. Lin, Y.-Y. Chen, Catal. Commun. 9 (2008) 2381-2385.
702 [49] P.-O. Larsson, A. Andersson, J. Catal. 179 (1998) 72-89.
703 [50] P.-O. Larsson, A. Andersson, L.R. Wallenberg, B. Svensson, J. Catal. 163 (1996) 279-
704 293.
705 [51] J. Li, G. Jacobs, T. Das, B.H. Davis, Appl. Catal. A: Gen. 233 (2002) 255-262.
706 [52] M.M. Yung, E.M. Holmgreen, U.S. Ozkan, J. Catal. 247 (2007) 356-367.
707 [53] K. Suriye, P. Praserthdam, B. Jongsomjit, Industrial & engineering chemistry research.
708 44 (2005) 6599-6604.
709 [54] W.S. Epling, P.K. Cheekatamarla, A.M. Lane, Chem. Eng. J. 93 (2003) 61-68.
710 [55] S.L. Soled, E. Iglesia, R.A. Fiato, G.B. Ansell, Google Patents, 1992.
711 [56] R. Riva, H. Miessner, R. Vitali, G. Del Piero, Appl. Catal. A: Gen. 196 (2000) 111-123.
712 [57] K. Jalama, N.J. Coville, D. Hildebrandt, D. Glasser, L.L. Jewell, J.A. Anderson, S.
713 Taylor, D. Enache, G.J. Hutchings, Top. Catal. 44 (2007) 129-136.
714 [58] K. Nagaoka, K. Takanabe, K.-i. Aika, Appl. Catal. A: Gen. 255 (2003) 13-21.
715 [59] Z. Zhao, M.M. Yung, U.S. Ozkan, Catal. Commun. 9 (2008) 1465-1471.
716 [60] Q. Yan, W. Weng, H. Wan, H. Toghiani, R. Toghiani, C. Pittman, Appl. Catal. A: Gen.
717 239 (2003) 43-58.
718 [61] S.-W. Ho, C.-Y. Chu, S.-G. Chen, J. Catal. 178 (1998) 34-48.
719 [62] J.T. Richardson, B. Turk, M. Lei, K. Forster, M.V. Twigg, Appl. Catal. A: Gen. 83
720 (1992) 87-101.
721 [63] P.K. de Bokx, R.L.C. Bonne, J.W. Geus, Applied Catalysis. 30 (1987) 33-46.
722 [64] M. Cubeiro, J. Fierro, Appl. Catal. A: Gen. 168 (1998) 307-322.
723 [65] R. Kam, C. Selomulya, R. Amal, J. Scott, J. Catal. 273 (2010) 73-81.

[66] N. Nava, T. Viveros, Hyperfine Interact. 122 (1999) 147-153.

[67] S.d.S. Corradini, G. Lenzi, M. Lenzi, C. Soares, O. Santos, J. Non-Cryst. Solids. 354 (2008) 4865-4870.

[68] Z. Wang, G. Zou, X. Luo, H. Liu, R. Gao, L. Chou, X. Wang, Journal of Natural Gas Chemistry. 21 (2012) 49-55.

[69] R. Burch, V. Caps, D. Gleeson, S. Nishiyama, S. Tsang, Appl. Catal. A: Gen. 194 (2000) 297-307.

[70] V. Deshmane, R. Abrokwah, D. Kuila, Int. J. Hydrogen Energy, (2015), http://dx.doi.org/10.1016/j.ijhydene.2015.06.084.

[71] F. Auprêtre, C. Descorme, D. Duprez, Catal. Commun. 3 (2002) 263-267.

Catalyst	**Surface Area (m^2/g)**	**Pore Size (nm)**	**Pore Volume (cm^3/g)**	**Actual Metal Loading (wt %) ICP-OES**	**TiO_2 Crystal Size (nm)**	**Metal Crystal Size (nm)**
TiO_2	146.6	3.59	0.172	0	17.18	-
10Cu-TiO_2	285.6	3.28	0.190	10.6	9.84	20.9
10Ni-TiO_2	309.8	3.32	0.203	13.9	-	-
10Co-TiO_2	215.1	3.30	0.142	13.3	4.03	-
10Sn-TiO_2	164.3	3.29	0.134	5.26	7.52	-
10Pd-TiO_2	99.7	3.32	0.081	5.32	8.78	49.4
10Zn-TiO_2	250.2	3.31	0.158	12.52	6.79	-
5Zn-TiO2	178.8	3.31	0.132	5.2	7.29	-
15Zn-TiO2	257.5	3.29	0.175	15.14	-	-
20Zn-TiO2	140.1	3.30	0.113	17.18	-	-

Table 1: Textural properties, actual metal loading and crystallite sizes of different M-TiO_2 catalyst samples